

Density functional approach to correlated moiré states: itinerant magnetism

Yang Zhang, Hiroki Isobe, and Liang Fu

Department of Physics, Massachusetts Institute of Technology, Cambridge, Massachusetts 02139, USA

Two-dimensional moiré superlattices have recently emerged as a fertile ground for creating novel electronic phases of matter with unprecedented control. Despite intensive efforts, theoretical investigation of correlated moiré systems has been challenged by the large number of atoms in a superlattice unit cell and the inherent difficulty of treating electron correlation. The physics of correlated moiré systems is governed by low-energy electrons in a coarse-grained long-wavelength potential, unlike the singular Coulomb potential of atomically-spaced ions in natural solids. Motivated by the separation between moiré and atomic length scales, in this work we apply density functional theory to study directly the continuum model of interacting electrons in the periodic moiré potential. Using this quantitatively accurate method, we predict itinerant spin-valley ferromagnetism in transition metal dichalcogenide heterobilayers, which originates from the constructive interplay between moiré potential and Coulomb interaction in a two-dimensional electron system.

Recent experiments on twisted bilayer graphene (TBG) [1–12], graphene-hBN heterostructures [13–16] and bilayer transition metal dichalcogenides (TMD) [17–19] uncovered a whole new world of strongly interacting electrons in moiré superlattices, forming a variety of correlated states such as unconventional superconductors and Chern insulators. From the theoretical point of view, an important task is to develop a systematic and quantitatively accurate method for tackling correlated electron states in moiré materials.

Despite the complexity associated with a large moiré unit cell containing $\sim 10,000$ atoms, the physics of correlated states in semimetal- or semiconductor-based moiré materials is governed by a small fraction of electrons (holes) near the conduction (valence) band edge. Here the relevant length scale far exceeds the interatomic distance, which justifies a continuum description based on effective field theory. A celebrated example is the non-interacting continuum model for TBG, which leads to the prediction of flat bands at the magic twist angle [20].

To treat electron interaction within the continuum theory, the Hartree–Fock (HF) approximation has been widely employed [21–26]. While it has yielded important insights on the insulating states in magic-angle graphene, the HF approximation often produces large errors in the ground-state energy and overestimate the tendency towards ferromagnetism. Moreover, the HF method is known to be ill-suited for treating metals, which are inherently unstable within this formalism. The lack of a reliable theoretical method hinders the study of correlated metallic states in moiré materials at generic fillings.

In this work, we introduce a density-functional-theory (DFT) based method for tackling correlated moiré states. Rather than including all the electrons of $\sim 10,000$ atoms in the moiré unit cell, we directly target low-energy electrons/holes under long-wavelength moiré potential, which form a two-dimensional Coulomb system described by the interacting continuum model. Our method combines the conceptual simplicity of continuum theory and the quantitative accuracy of DFT. It is predictive, efficient and versatile.

Applying this “moiré-DFT” method to TMD heterobi-

layers such as WSe_2/WS_2 , we find that at large moiré period, the ground state in a range of fillings around $n = 1.3$ holes per unit cell is an itinerant ferromagnet with full spin-valley polarization. By tracking the ground state energy as a function of the moiré potential strength and the filling, we show that the itinerant ferromagnetism originates from the constructive interplay between Coulomb interaction and the periodic moiré potential, which goes beyond the scope of single-band Hubbard model.

Our results shed light on a recent optical experiment on hole-doped WSe_2/WS_2 suggesting a possible transition between distinct ground-state magnetic orders around the filling $n = 1.2$ [17]. Based on moiré-DFT calculations, we find the critical twist angle for the onset of itinerant ferromagnetism, and propose transport and spectroscopic experiments for its detection.

Monolayer TMDs such as WSe_2 , WS_2 , MoS_2 and MoSe_2 are semiconductors with a direct band gap located at K and K' points of the Brillouin zone. Due to spin-valley locking, holes at K and K' valleys carry opposite out-of-plane spins denoted by $s_z = \uparrow, \downarrow$. The energy dispersions of holes in the two valleys are identical within the effective mass approximation. In a TMD heterobilayer WSe_2/WS_2 , holes in the WSe_2 layer experience a long-wavelength periodic potential $V(\mathbf{r})$ introduced by the WS_2 layer due to the 4% lattice mismatch. Thus, the continuum Hamiltonian for hole-doped TMD heterobilayers takes the general form

$$\mathcal{H} = \sum_i \left(-\frac{\nabla_i^2}{2m} + V(\mathbf{r}_i) \right) + \frac{1}{2} \sum_{j \neq i} \frac{k_e e^2}{\epsilon |\mathbf{r}_i - \mathbf{r}_j|}, \quad (1)$$

where m is the effective hole mass (about $0.5m_e$ for WSe_2 [18, 27, 28]), and $k_e = 1/(4\pi\epsilon_0)$ is Coulomb constant. Here m_e is the electron mass and ϵ_0 is the vacuum permittivity. The dielectric constant of the electrostatic environment ϵ is estimated to be $\epsilon \sim 6$ when hexagonal boron nitride is used as the substrate [29].

Since the moiré potential $V(\mathbf{r})$ is smooth and has the triangular lattice symmetry, it can be parameterized us-

ing the three lowest Fourier components [30]:

$$V(\mathbf{r}) = -2V_0 \sum_{l=1}^3 \cos(\mathbf{G}_l \cdot \mathbf{r} + \phi), \quad (2)$$

where $\mathbf{G}_l = \frac{4\pi}{\sqrt{3}L_m} (\cos \frac{2\pi l}{3}, \sin \frac{2\pi l}{3})$ are the reciprocal vectors of the moiré superlattice. The moiré period L_m increases as the twist angle θ decreases, reaching 8.2 nm for WSe₂/WS₂ at $\theta = 0$ (aligned). The values of V_0, ϕ for various TMD heterobilayers have been obtained from our all-electron DFT calculation at charge neutrality [31]. For WSe₂/WS₂, $V_0 = 15\text{meV}$ and $\phi \approx \pi/4$.

The continuum Hamiltonian defined by (1) and (2) is the starting point of our study. It is instructive to recast \mathcal{H} in dimensionless form:

$$\mathcal{H}/E_0 = \sum_i \left(-\frac{\tilde{\nabla}_i^2}{2} - v_0(\tilde{\mathbf{r}}) \right) + \frac{1}{2} \sum_{j \neq i} \frac{Z}{|\tilde{\mathbf{r}}_i - \tilde{\mathbf{r}}_j|}, \quad (3)$$

where we define $\tilde{\mathbf{r}} \equiv \mathbf{r}/L_m$ and $E_0 \equiv \hbar^2/(mL^2)$. The

dimensionless parameter $v_0 \equiv V_0/E_0$ characterizes the moiré potential strength relative to the kinetic energy, while the ratio of moiré period and the effective Bohr radius $a_B = 4\pi\epsilon_0\epsilon\hbar^2/(me^2)$ defines the dimensionless Coulomb interaction parameter $Z \equiv L_m/a_B$. The ground state thus depends on three dimensionless parameters: v_0, Z , and the filling factor $n = \frac{\sqrt{3}}{2}\rho L_m^2$ where ρ is the hole density. This makes TMD heterobilayers a highly-tunable two-dimensional hole system. Varying the moiré period with the twist angle and the hole density via gating can span the full range between weak and strong interaction and between weak and strong potential, thus promising a plethora of electronic states to be discovered.

We now apply the Kohn–Sham density functional theory[32] to the 2D periodic electron system defined by the continuum Hamiltonian (1). The essence of the DFT method is to find the ground state total energy E and spin densities $n_\uparrow(\mathbf{r}), n_\downarrow(\mathbf{r})$ of an interacting system by solving an auxiliary one-body Schrödinger equation:

$$\left(-\frac{\nabla^2}{2m} + V(\mathbf{r}) + U([n], \mathbf{r}) + \frac{\delta E_{xc}([n_\uparrow, n_\downarrow])}{\delta n_\sigma(\mathbf{r})} \right) \psi_{i\sigma}(\mathbf{r}) = \epsilon_{i\sigma} \psi_{i\sigma}(\mathbf{r}) \quad \text{and} \quad n_\sigma(\mathbf{r}) = \sum_i \theta(\mu - \epsilon_{i\sigma}) |\psi_{i\sigma}(\mathbf{r})|^2, \quad (4)$$

where $i\sigma$ denotes a complete set of single-particle orbitals (Kohn–Sham orbitals). Here, in addition to the external potential, the effective potential includes the Hartree potential U and the spin-dependent potential $\frac{\delta E_{xc}([n_\uparrow, n_\downarrow])}{\delta n_\sigma(\mathbf{r})}$. The former is associated with classical electrostatic energy of the inhomogeneous charge density

$$U([n], \mathbf{r}) = \frac{e^2}{\epsilon} \int d\mathbf{r}' \frac{n(\mathbf{r}')}{|\mathbf{r} - \mathbf{r}'|}, \quad n(\mathbf{r}) = n_\uparrow(\mathbf{r}) + n_\downarrow(\mathbf{r}). \quad (5)$$

The latter depends on the exchange-correlation energy E_{xc} , which is a functional of spin-dependent density $n_\sigma(\mathbf{r})$. Since the effective potential itself relies on the spin density of occupied Kohn–Sham orbitals, we should solve the above equation iteratively until reaching the self-consistency.

DFT is exact in principle, but in practice it requires an approximation to the exchange-correlation energy functional. In this work, we use the local spin density functional (LSD) approximation[32–34]

$$E_{xc}([n_\uparrow, n_\downarrow]) = \int d\mathbf{r} n(\mathbf{r}) \epsilon_{xc}(n_\uparrow(\mathbf{r}), n_\downarrow(\mathbf{r})). \quad (6)$$

$\epsilon_{xc}(n_\uparrow, n_\downarrow)$ is the exchange-correlation energy per particle in a *two-dimensional* electron gas with uniform spin densities n_\uparrow, n_\downarrow . In the following we use the function ϵ_{xc} obtained by Attaccalite *et al* from quantum Monte Carlo simulations [35]. By construction, the LSD

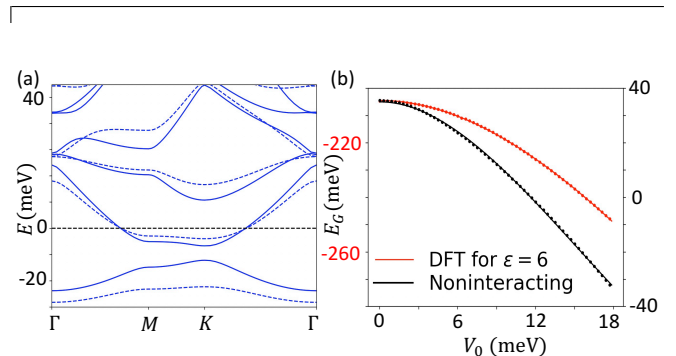


FIG. 1: (a) Band structure the metallic ground state at the filling $n = 3$ for $L_m = 8.2\text{ nm}$, $\phi = 45^\circ$, obtained from DFT calculation at $\epsilon = 6$ (solid line) and non-interacting continuum model (dashed line). (b) The ground-state energy per unit cell as a function of potential strength, fitted with a fourth-order polynomial.

approximation[36–39] is exact for homogeneous systems. In practice, DFT with the LSD approximation has proven to be accurate for a wide variety of inhomogeneous systems: atoms, molecules and natural solids including metals and itinerant ferromagnets [40, 41].

We perform DFT calculations under LSD approximation on the continuum Hamiltonian (1,2) for TMD heterobilayer WSe₂/WS₂, at various charge densities and moiré periods L_m . When the charge density is relatively high, we find that Coulomb interaction renormalizes the

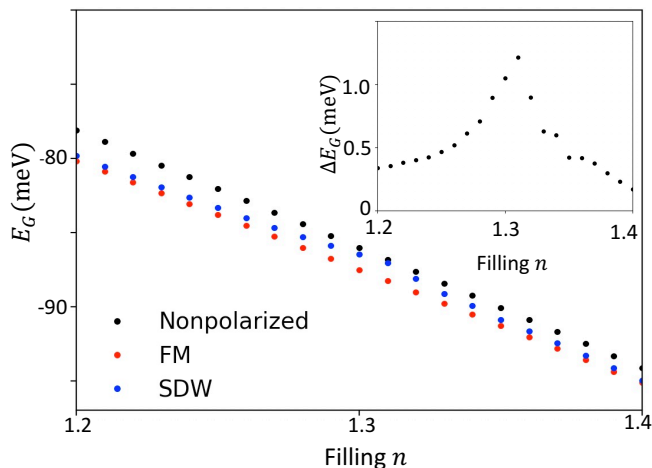


FIG. 2: The ground-state energy per unit cell of fully-polarized state, spin-density-wave state, and non-spin-polarized state as a function of filling, calculated for $L_m = 8.2\text{nm}$, $V_0 = 15\text{meV}$, $\phi = 45^\circ$ and $\epsilon = 6$. The inset shows the energy difference between SDW state and FM state: $\Delta E_G = E_G(\text{SDW}) - E_G(\text{FM})$.

metallic states at generic fillings without making qualitative changes. As an example, Figure 1(a) shows the DFT band structure for aligned WSe_2/WS_2 at the filling of $n = 3$ holes per moiré unit cell, corresponding to a hole density $\rho = 5.15 \times 10^{12} \text{cm}^{-2}$. We further calculate the ground-state energy E_G as a function of the moiré potential strength V_0 , finding an excellent fit with a fourth-order polynomial, see Fig. 2(a). This dependence, as expected from a perturbation expansion in $V(\mathbf{r})$, proves that the metallic ground state at $V_0 = 15 \text{meV}$ (the parameter for WSe_2/WS_2) is adiabatically connected to the homogeneous hole gas without the moiré potential.

We also compare the energies and charge distributions of the metallic state at $n = 3$ with and without Coulomb interaction. Compared to the non-interacting case, the charge distribution at $\epsilon = 6$ has less spatial variation, as expected from the Coulomb energy cost associated with charge inhomogeneity. These results on renormalized metal serves as a benchmark of our DFT method.

We now turn to the strongly correlated regime of TMD heterobilayers at large moiré wavelength and low density. For aligned WSe_2/WS_2 with $L_m = 8.2 \text{nm}$, our spin-dependent DFT calculations reveal that the ground state at fillings between $n = 1.2$ and 1.4 is a fully spin-polarized metal. At a given hole density ρ , our calculation starts from random initial spin densities $n_\uparrow(\mathbf{r})$ and $n_\downarrow(\mathbf{r})$ with average values $\bar{n}_\uparrow = \bar{n}_\downarrow = \rho/2$. The iteration of the Kohn–Sham equation (4) always converges to a fully spin-polarized ground state.

For comparison, when we enforce $n_\uparrow(\mathbf{r}) = n_\downarrow(\mathbf{r})$ everywhere in solving the Kohn–Sham equation, a non-spin-polarized solution is obtained, but its energy is higher than the fully polarized state. We further investigate the possibility of translational symmetry breaking by per-

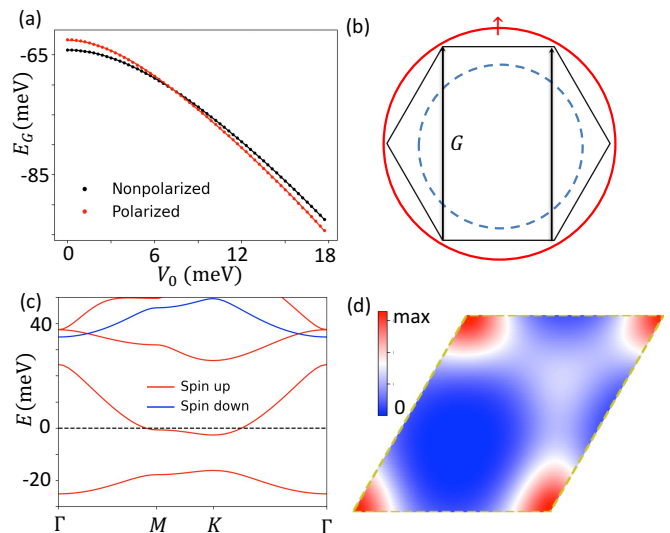


FIG. 3: Itinerant ferromagnet at the filling $n = 1.3$ for $L_m = 8.2\text{nm}$ and $\phi = 45^\circ$. (a) The ground-state energy per unit cell as a function of the moiré potential strength V_0 ; (b) The Fermi surfaces of the non-polarized (blue) and fully-polarized uniform electron gas (red) at the density of $n = 1.3$ electrons per unit cell, in comparison with the Brillouin zone (hexagon). (c) DFT band structure and (d) Real-space charge distribution of the fully-polarized state.

forming spin-dependent DFT calculations with a 2×1 enlarged unit cell. Starting from random initial spin densities, we find that the majority of iterations converge to the fully-polarized metal described above, while in some cases a metallic state with spin stripe order is obtained.

Fig.2 shows the filling-dependent ground-state energies of the fully-polarized state, the spin-density wave state, and the (enforced) non-magnetic state. Importantly, within the filling range $1.2 < n < 1.4$, the fully-polarized state is always found to have the lowest energy, while the non-magnetic state has the highest energy. Their energy difference, which measures the energy gain from itinerant ferromagnetism, decreases monotonically as the hole density increases. On the other hand, at fillings close to 1.2 or 1.4 , the fully-polarized state and the spin-density-wave state become extremely close in energy, indicating a competition between distinct magnetic orders. The ferromagnetic ground state is the most stable around the filling $n = 1.3$, where its energy per unit cell is lower than the other states by $> 1\text{meV}$.

To gain insight into the origin of itinerant ferromagnetism, we calculate and compare the ground-state energies of fully-polarized ($\zeta = 1$) and non-polarized ($\zeta = 0$) states at the filling $n = 1.3$, as a function of the potential strength V_0 . Here $\xi \equiv (N_\uparrow - N_\downarrow)/(N_\uparrow + N_\downarrow)$ denotes the spin polarization. As shown in Figure 3(a), $E^{\zeta=1,0}(V_0)$ fit nicely with fourth-order polynomials, which proves the adiabatic continuity to the uniform hole gas at $V_0 = 0$, with full and zero spin polarization respectively.

At $V_0 = 0$, the non-polarized uniform hole gas has a

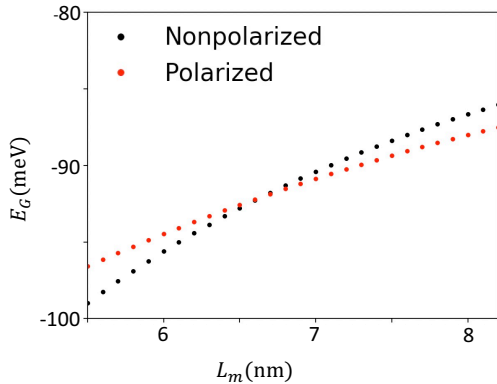


FIG. 4: The ground-state energy per unit cell of the fully-polarized and non-polarized state as a function of the moiré period, at the filling $n = 1.3$, $V_0 = 15$ meV, and $\phi = 45^\circ$

lower energy. However, due to the large effective mass and low density (the corresponding interaction parameter is $r_s = 5.35$), its spin susceptibility is strongly enhanced by Coulomb interaction, making its energy difference with the fully-polarized state relatively small. At the hole density corresponding to the filling $n = 1.3$, the Fermi surface in the fully-polarized case lies just slightly outside the first Brillouin zone (a hexagon), and in the non-polarized case falls entirely within it, i.e., $2k_F^{\xi=0} < G < 2k_F^{\xi=1}$ as shown in Fig. 2(d). Since the density wave susceptibility of a uniform hole gas decreases rapidly at wavevectors greater than $2k_F$, the fully-polarized state exhibits a larger density response to the moiré potential, hence lowers its energy faster with increasing potential strength, and eventually becomes the true ground state above a critical V_0 .

The electronic structure and real-space charge distribution of the ferromagnetic (FM) metal at $n = 1.3$ are shown in Fig. 1(c) and (d) respectively. The lowest moiré band, completely filled by spin-polarized holes, give rise to one $s = 1/2$ local moment in the AA region of each moiré unit cell. The remaining 0.3 holes per unit cell partially occupy the second moiré band, and are distributed primarily in the AB region, consistent with the strong-coupling picture of $n - 1$ doped holes being transferred to AB orbitals to avoid double occupancy of AA orbitals [31]. It is worth emphasizing that in the ferromagnetic metal we found at $n > 1$, the (pseudo-)spins of *all* holes are aligned, resulting in n pseudospin-1/2 magnetic moment per moiré unit cell, whereas the density of mobile charge carriers is $n - 1$. This behavior cannot be captured by any single-band Hubbard model, which can accommodate at most $2 - n$ spins per unit cell at $n > 1$.

We further show that itinerant ferromagnetism in TMD heterobilayers is tunable by increasing the twist angle θ to reduce the moiré period L_m . A smaller L_m leads to a larger bandwidth and hence weakens electron correlation. Figure 4 shows the energies of the FM state and

the non-magnetic state as a function of L_m . A quantum phase transition from the FM state to the non-magnetic state occurs at $L_m \approx 6.5$ nm, or $\theta \approx 1.75^\circ$.

We now compare our findings with a recent optical experiment on hole-doped WSe_2/WS_2 , which observed Curie-Weiss behavior in the temperature dependence of the exciton Zeeman splitting. Remarkably, above the filling $n = 1.2$, the Weiss constant changes sign from negative to positive, consistent with a ferromagnetic metal we found between $n = 1.2$ and 1.4. To establish ferromagnetism in WSe_2/WS_2 , it is desirable to measure the magnetization as a function of the filling by SQUID. The reduced density $n - 1$ of mobile holes in the FM metal can be measured in Hall and quantum oscillation experiments. The complete removal of spin degeneracy can be directly tested from the Landau level fan diagram.

At nonzero temperature, thermal fluctuations destroy long-range FM order in two dimensional systems with the continuous spin-rotational symmetry. For TMD heterobilayers, however, magnetic dipole-dipole interaction or higher-order valley-contrasting energy dispersion such as $(k_x^3 - 3k_x k_y^2)s_z$, is expected to result in uniaxial magnetic anisotropy and thus stabilize the itinerant ferromagnetism at low temperature. If the z direction is the easy axis, the FM metal has a spontaneous out-of-plane magnetization, which can be detected by anomalous Hall effect or magnetic circular dichroism. Alternatively, an easy-plane anisotropy will lead to an inter-valley coherent state, which is expected to enable superfluid-like spin transport [42, 43]. Thus, TMD moiré superlattices provide a new and highly tunable platform for the study of fundamental mechanism of itinerant magnetism in two dimensions, and may enable the design of electrically controllable spintronics devices [44–46].

To summarize, our DFT calculations reveal itinerant ferromagnetism stabilized by the moiré potential in a two-dimensional Coulomb system, the TMD-based moiré superlattices. This finding, which goes beyond the scope of single-band Hubbard model, demonstrates the predictive power of our moiré-DFT method targeting directly low-energy electrons in a coarse-grained moiré potential. This method will discover a variety of broken-symmetry states in TMD heterobilayers at other fillings, thus guiding future experiments. Its capability will be further extended by improvements in the exchange-correlation functional to handle Dirac electrons in graphene-based moiré systems. We hope that moiré-DFT becomes a useful tool for the investigation of many-electron physics in all moiré materials.

Acknowledgment

We thank Kin Fai Mak, Jie Shan and Feng Wang for numerous discussions on experiments, and Allan MacDonald for valuable theoretical discussions.

-
- [1] Y. Cao, V. Fatemi, A. Demir, S. Fang, S. L. Tomarken, J. Y. Luo, J. D. Sanchez-Yamagishi, K. Watanabe, T. Taniguchi, E. Kaxiras, et al., *Nature* **556**, 80 (2018).
- [2] Y. Cao, V. Fatemi, S. Fang, K. Watanabe, T. Taniguchi, E. Kaxiras, and P. Jarillo-Herrero, *Nature* **556**, 43 (2018).
- [3] X. Lu, P. Stepanov, W. Yang, M. Xie, M. A. Aamir, I. Das, C. Urgell, K. Watanabe, T. Taniguchi, G. Zhang, et al., *Nature* **574**, 653 (2019).
- [4] A. Kerelsky, L. J. McGilly, D. M. Kennes, L. Xian, M. Yankowitz, S. Chen, K. Watanabe, T. Taniguchi, J. Hone, C. Dean, et al., *Nature* **572**, 95 (2019).
- [5] Y. Jiang, X. Lai, K. Watanabe, T. Taniguchi, K. Haule, J. Mao, and E. Y. Andrei, *Nature* **573**, 91 (2019).
- [6] Y. Xie, B. Lian, B. Jäck, X. Liu, C.-L. Chiu, K. Watanabe, T. Taniguchi, B. A. Bernevig, and A. Yazdani, *Nature* **572**, 101 (2019).
- [7] Y. Choi, J. Kemmer, Y. Peng, A. Thomson, H. Arora, R. Polski, Y. Zhang, H. Ren, J. Alicea, G. Refael, et al., *Nature Physics* **15**, 1174 (2019).
- [8] M. Yankowitz, S. Chen, H. Polshyn, Y. Zhang, K. Watanabe, T. Taniguchi, D. Graf, A. F. Young, and C. R. Dean, *Science* **363**, 1059 (2019).
- [9] E. Codecido, Q. Wang, R. Koester, S. Che, H. Tian, R. Lv, S. Tran, K. Watanabe, T. Taniguchi, F. Zhang, et al., *Science Advances* **5**, eaaw9770 (2019).
- [10] A. L. Sharpe, E. J. Fox, A. W. Barnard, J. Finney, K. Watanabe, T. Taniguchi, M. Kastner, and D. Goldhaber-Gordon, *Science* **365**, 605 (2019).
- [11] S. Tomarken, Y. Cao, A. Demir, K. Watanabe, T. Taniguchi, P. Jarillo-Herrero, and R. Ashoori, *Physical review letters* **123**, 046601 (2019).
- [12] U. Zondiner, A. Rozen, D. Rodan-Legrain, Y. Cao, R. Queiroz, T. Taniguchi, K. Watanabe, Y. Oreg, F. von Oppen, A. Stern, et al., arXiv preprint arXiv:1912.06150 (2019).
- [13] G. Chen, L. Jiang, S. Wu, B. Lyu, H. Li, B. L. Chittari, K. Watanabe, T. Taniguchi, Z. Shi, J. Jung, et al., *Nature Physics* **15**, 237 (2019).
- [14] G. Chen, A. L. Sharpe, P. Gallagher, I. T. Rosen, E. J. Fox, L. Jiang, B. Lyu, H. Li, K. Watanabe, T. Taniguchi, et al., *Nature* **572**, 215 (2019), URL <https://doi.org/10.1038/s41586-019-1393-y>.
- [15] M. Serlin, C. Tschirhart, H. Polshyn, Y. Zhang, J. Zhu, K. Watanabe, T. Taniguchi, L. Balents, and A. Young, *Science* (2019).
- [16] X. Liu, Z. Hao, E. Khalaf, J. Y. Lee, K. Watanabe, T. Taniguchi, A. Vishwanath, and P. Kim, arXiv preprint arXiv:1903.08130 (2019).
- [17] Y. Tang, L. Li, T. Li, Y. Xu, S. Liu, K. Barmak, K. Watanabe, T. Taniguchi, A. H. MacDonald, J. Shan, et al., *Nature* **579**, 353 (2020).
- [18] E. C. Regan, D. Wang, C. Jin, M. I. B. Utama, B. Gao, X. Wei, S. Zhao, W. Zhao, Z. Zhang, K. Yumigeta, et al., *Nature* **579**, 359 (2020).
- [19] L. Wang, E.-M. Shih, A. Ghiotto, L. Xian, D. A. Rhodes, C. Tan, M. Claassen, D. M. Kennes, Y. Bai, B. Kim, et al., arXiv preprint arXiv:1910.12147 (2019).
- [20] R. Bistritzer and A. H. MacDonald, *Proceedings of the National Academy of Sciences* **108**, 12233 (2011).
- [21] F. Guinea and N. R. Walet, *Proceedings of the National Academy of Sciences* **115**, 13174 (2018).
- [22] T. Cea, N. R. Walet, and F. Guinea, *Physical Review B* **100**, 205113 (2019).
- [23] M. Xie and A. H. MacDonald, *Physical Review Letters* **124**, 097601 (2020).
- [24] N. Bultinck, E. Khalaf, S. Liu, S. Chatterjee, A. Vishwanath, and M. P. Zaletel, arXiv preprint arXiv:1911.02045 (2019).
- [25] J. Liu and X. Dai, arXiv preprint arXiv:1911.03760 (2019).
- [26] Y. Zhang, K. Jiang, Z. Wang, and F. Zhang, arXiv preprint arXiv:2001.02476 (2020).
- [27] B. Fallahazad, H. C. Movva, K. Kim, S. Larentis, T. Taniguchi, K. Watanabe, S. K. Banerjee, and E. Tutuc, *Physical review letters* **116**, 086601 (2016).
- [28] F. A. Rasmussen and K. S. Thygesen, *The Journal of Physical Chemistry C* **119**, 13169 (2015).
- [29] A. V. Stier, N. P. Wilson, G. Clark, X. Xu, and S. A. Crooker, *Nano letters* **16**, 7054 (2016).
- [30] F. Wu, T. Lovorn, E. Tutuc, and A. H. MacDonald, *Physical review letters* **121**, 026402 (2018).
- [31] Y. Zhang, N. F. Yuan, and L. Fu, arXiv preprint arXiv:1910.14061 (2019).
- [32] W. Kohn and L. J. Sham, *Physical review* **140**, A1133 (1965).
- [33] U. von Barth and L. Hedin, *Journal of Physics C: Solid State Physics* **5**, 1629 (1972).
- [34] A. Rajagopal and J. Callaway, *Physical Review B* **7**, 1912 (1973).
- [35] C. Attacalite, S. Moroni, P. Gori-Giorgi, and G. B. Bachelet, *Physical review letters* **88**, 256601 (2002).
- [36] S. H. Vosko, L. Wilk, and M. Nusair, *Canadian Journal of physics* **58**, 1200 (1980).
- [37] J. P. Perdew and A. Zunger, *Physical Review B* **23**, 5048 (1981).
- [38] L. A. Cole and J. Perdew, *Physical Review A* **25**, 1265 (1982).
- [39] J. P. Perdew and Y. Wang, *Physical Review B* **45**, 13244 (1992).
- [40] V. Moruzzi, J. Janak, and A. Williams (1978).
- [41] J. Sticht, K. Höck, and J. Kübler, *Journal of Physics: Condensed Matter* **1**, 8155 (1989).
- [42] Z. Bi and L. Fu, arXiv preprint arXiv:1911.04493 (2019).
- [43] C. Jin, J. Kim, M. I. B. Utama, E. C. Regan, H. Kleemann, H. Cai, Y. Shen, M. J. Shinner, A. Sengupta, K. Watanabe, et al., *Science* **360**, 893 (2018).
- [44] B. Huang, G. Clark, D. R. Klein, D. MacNeill, E. Navarro-Moratalla, K. L. Seyler, N. Wilson, M. A. McGuire, D. H. Cobden, D. Xiao, et al., *Nature nanotechnology* **13**, 544 (2018).
- [45] S. Jiang, L. Li, Z. Wang, K. F. Mak, and J. Shan, *Nature nanotechnology* **13**, 549 (2018).
- [46] A. Manchon, J. Železný, I. M. Miron, T. Jungwirth, J. Sinova, A. Thiaville, K. Garello, and P. Gambardella, *Reviews of Modern Physics* **91**, 035004 (2019).